NANO LETTERS

Letter

pubs.acs.org/NanoLett

Size-Dependent Deformation of Nanocrystalline Pt Nanopillars

X. Wendy Gu,[†] Colleen N. Loynachan,[⊥] Zhaoxuan Wu,[§] Yong-Wei Zhang,[§] David J. Srolovitz,[§,∥] and Julia R. Greer*[,‡,#]

[†]Division of Chemistry and Chemical Engineering, [‡]Division of Engineering and Applied Sciences, [#]The Kavli Nanoscience Institute, California Institute of Technology, 1200 E. California Blvd., Pasadena, California 91125, United States

[⊥]Department of Materials Science and Engineering, Massachusetts Institute of Technology, 77 Massachusetts Avenue, Cambridge, Massachusetts 02139, United States

[§]Institute of High Performance Computing, 1 Fusionopolis Way, #16-16 Connexis, Singapore 138632

[∥]Departments of Materials Science and Engineering & Mechanical Engineering and Applied Mechanics, University of Pennsylvania, Philadelphia, Pennsylvania 19104, United States

Supporting Information

ABSTRACT: We report the synthesis, mechanical properties, and deformation mechanisms of polycrystalline, platinum nanocylinders of grain size d = 12 nm. The number of grains across the diameter, D/d, was varied from 5 to 80 and 1.5 to 5 in the experiments and molecular dynamics simulations, respectively. An abrupt weakening is observed at a small D/d, while the strengths of large nanopillars are similar to bulk. This "smaller is weaker" trend is opposite to the "smaller is stronger" size effect in single crystalline nanostructures. The simulations demonstrate that the size-dependent behavior is associated with the distinct deformation mechanisms operative in interior versus surface grains.

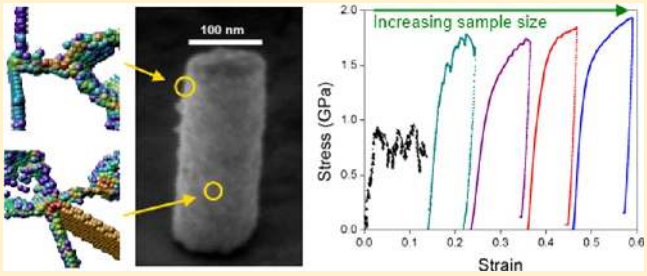

KEYWORDS: *Size effect, nanocrystalline, mechanical properties, molecular dynamics*

The control of material properties through manipulation of microstructural length scales is standard practice among material scientists and engineers. Grain refinement generally leads to improved material strength, as described, for example, by the Hall–Petch relation.[1,2] Recently, sample size (an extrinsic length scale) has emerged as another controlling factor in the mechanical behavior of metals when the sample size is reduced to the micrometer scale and below.[3,4] Monolithic single crystalline pillars with diameters spanning tens of nanometers to tens of micrometers have been shown to exhibit an order of magnitude increase in strength over bulk in uniaxial compression and tension testing. This "smaller is stronger" trend has been reported for a wide variety metals (e.g., Ni, Au, Cu, Mo, W, Nb, V, and Ta) and in samples fabricated by techniques ranging from focused ion beam (FIB) milling of individual pillars to top-down techniques such as electroplating into a template and embossing using a mold.[3−8] The deformation mechanisms in these small-scale samples have been demonstrated to fundamentally differ from those in the same metals with macroscopic dimensions because of the influence of free surfaces on dislocation behavior. For example, in face-centered cubic (fcc) single crystalline metals, dislocations are generated by the operation of the so-called single arm dislocation sources in micrometer-sized structures and via dislocation nucleation at surfaces in nanometer-sized structures.[9,10] Another unique aspect of small-scale deformation of single crystals is that the stress–strain curves are punctuated by discrete bursts, corresponding to dislocation avalanches.[11]

Most research efforts on small-scale mechanical behavior to date have focused on single crystalline nanopillars; however, some ongoing and recent investigations focused on the effects of interfaces within nanostructures (grain boundaries, twin boundaries, and bimaterial interfaces) on the mechanical response.[12−20] Understanding the fracture and yield strengths of nanostructures containing multiple grain boundaries as a function of sample dimensions is particularly important for the design of reliable nanoelectromechanical system (NEMS) and microelectromechanical system (MEMS) devices, in which nanometer feature sizes are common constituents of more heterogeneous microstructures. Some studies on the strengths of nanocrystalline fcc nanostructures have been conducted; for example, the effects of size on the deformation of 7-, 30-, and 60-nm grained Ni and Ni–W have been reported.[16,17,21] Jang and Greer observed a "smaller is weaker" trend in the grain boundary-mediated deformation of a Ni-4%W alloy with grain size d = 60 nm and sample dimensions spanning 2 orders of magnitude.[16] Rinaldi et al. observed a marginal increase in the compressive strengths of d = 30 nm Ni pillars with increasing

Received: October 5, 2012
Revised: November 11, 2012
Published: November 13, 2012

   dx.doi.org/10.1021/nl3036993 | *Nano Lett.* 2012, 12, 6385−6392

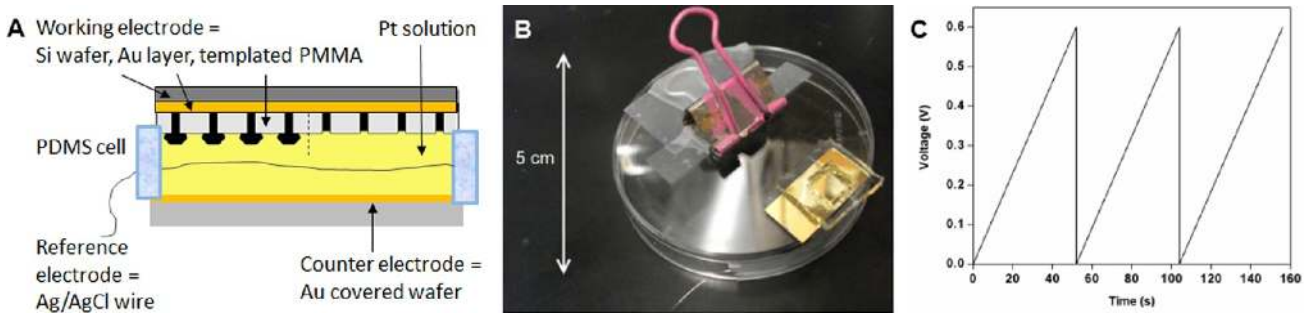

Figure 1. Electroplating setup employed to deposit the samples: (A) a schematic of the three-electrode electrochemical cell and (B) a photograph of electrochemical cell mounted on a Petri dish. (C) Representative electroplating sawtooth voltage−time plot where the voltage is repeatedly cycled from 0 to 0.6 V.

pillar diameter, D, from ∼160 to 272 nm.[17] All of those samples contained 2−40 grains across the nanopillar diameter. It is apparent that a wider range of materials, sample-to-grain size ratios D/d, and sample geometries should be systematically investigated to gain a clear understanding of the transition from the internal length-scale dominated deformation of larger samples to the smaller length-scale regime where intrinsic (microstructure) and extrinsic (sample size) length-scales compete.

Specimens with few grains across the diameter have previously been studied at the macro and the micro scale. It was reported that weakening occurs below a critical sample size to grain size ratio due to the lower resistance to dislocation activity within grains at free surfaces.[22−25] It is unclear whether this size-induced weakening extends to the nanoscale because dislocations may not be the main carriers of plastic deformation in nanograined metals.[26−28] Bulk nanocrystalline metals with grain sizes below ∼30 nm have been shown to exhibit reduced strength with decreased grain size.[26] The precise mechanistic source of this so-called inverse Hall−Petch effect is a matter of ongoing discussion. The candidate mechanisms include grain boundary rotation, sliding, migration, and the operation of partial dislocations nucleated at grain boundaries.[27−30] The study of nanocrystalline metals of composition and size beyond the most widely studied (Ni, Cu, and Co) will help sort out the origins of this widely observed inverse Hall−Petch regime.

In this work, we explored the effect of external sample size on the deformation of platinum nanopillars of fixed grain size, d = 12 nm. Nanostructured Pt is widely used in technological devices and catalysis for energy generation and pollution reduction and is especially suitable for nanomechanical testing because of its minimal oxide formation.[31] The nanopillars contained, on average, 5−80 grains across the 60−1000 nm cylindrical sample diameters. Molecular dynamics simulations were performed on an overlapping range of sample diameters, $22 \leq D \leq 64$ nm (i.e., $1.5 \leq D/d \leq 5$), and for similar height-to-width nanopillar aspect ratios. The Pt grain structures in the simulated nanopillars were constructed to mimic those used in the experiments. Microstructural transmission electron microscopy (TEM) analysis revealed that the Pt nanostructures contained few or no initial dislocations, so dislocations were not introduced into the as-constructed polycrystalline nanopillars used in the simulations.

Nanocrystalline Pt nanopillars with diameters from approximately 60 nm to 1 μm were formed by electroplating into an electron-beam lithography patterned poly(methyl methacrylate) (PMMA) template, fabricated following the methodology of Burek and Greer.[32] In addition, 1.5-μm-thick nanocrystalline Pt films were electroplated onto 100 × 100 μm^2 rectangular electrodes formed using a nanometer pattern generator system (FEI Quanta 600F) to create openings in the PMMA layer on an Au-covered silicon wafer. The films were produced for measurement of the yield stress of bulk nanocrystalline Pt with grain sizes identical to that of the nanopillars. The electroplating was performed using a three-electrode electrochemical cell with an Ag/AgCl pseudoreference electrode, a gold counter electrode, the patterned template as the working electrode and walls made of cured polydimethylsiloxane[33] (see Figure 1A and B). This process was developed specifically for the fabrication of nanocrystalline Pt and is distinct from the commonly used electroplating methodology.[6,32] The electrochemical cell was designed to use only 0.1 mL of the electroplating bath for safety and economy. The Pt electroplating solution consisted of 10 mM chloroplatinic acid (Alfa Aesar) and 0.5 M sulfuric acid (Mallinckrodt Chemicals) in deionized water.[34] Plating process development and optimization revealed that a sawtoothed electrodeposition scheme produced void-free, uniform structures (see Figure 1C and Table 1). The voltage is repeatedly increased linearly from the initial to final voltage at a set rate according to the conditions in Table 1 until structures of a desired height and geometry are achieved (see Figure 2A−C).

Table 1. Electroplating Conditions

diameter/thickness (nm)	initial voltage (V)	final voltage (V)	ramp rate (mV/s)
60 ± 2	0	0.4	57
113 ± 1, 261 ± 7	0	0.6	86
472 ± 10, 986 ± 18, thin film	0	0.5	36

The microstructure was examined using TEM (TF20, FEI Co.) operating at 200 kV, as shown in Figure 2D and E. The 60-nm-thick samples with over electroplated "heads" were transferred from the growth substrate to a Cu TEM grid by attaching an Omniprobe micromanipulator to the head with electrostatic forces. This TEM sample preparation method did not require additional thinning and avoided exposure to the focused ion beam (FIB) and the ensuing radiation damage. The larger diameter pillars (and the underlying silicon) were milled from the substrate using FIB and transferred onto a Cu TEM grid using an Omniprobe micromanipulator to prepare for TEM analysis. Once on the grid, these larger nanopillars were thinned to an electron-transparent thickness (less than 100 nm) using the FIB at the lowest available current setting (10 pA and 30 kV accelerating voltage). The average grain size was identified to be 12 ± 4 nm based on TEM dark field images

dx.doi.org/10.1021/nl3036993 | Nano Lett. 2012, 12, 6385−6392

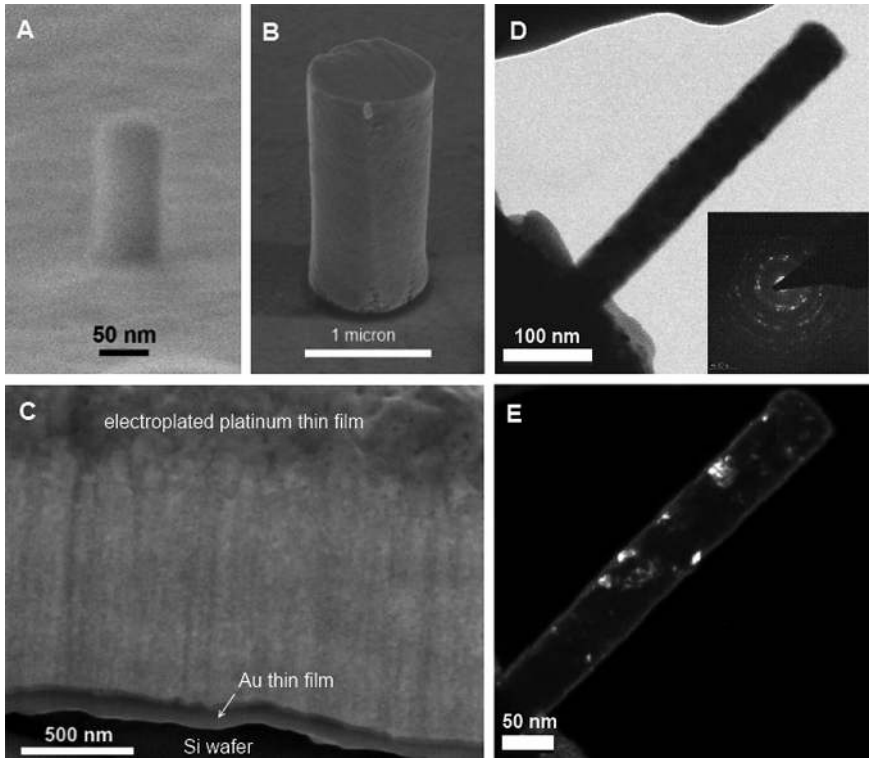

Figure 2. Electroplated nanocrystalline Pt nanostructures. Scanning electron microscopy (SEM) images of (A) 60 nm wide pillar (image taken at 86° tilt), (B) 1 μm wide pillar with top surface smoothed by a focused ion beam (FIB, 52° tilt), and (C) a cross-section of a 1.5-μm-thick film (52° tilt). TEM images of 60 nm wide pillar in (D) a bright field with corresponding diffraction pattern as the inset, and (E) dark field image used to determine grain sizes.

(Figure 2E). TEM analysis revealed well-formed grains, grain boundaries, and triple-junctions (the lines along which three grains meet).

Uniaxial compression testing of the 60 nm diameter pillars was conducted in the SEMentor, a combined scanning electron microscope (SEM) and nanoindenter (Nanomechanics, Inc.) using a custom-made flat punch tip at a nominal strain rate of 0.001/s. The small pillar required the determination of the precise location of the pillar using SEM to ensure alignment of the pillar and the nanoindenter tip. All other samples were tested in the G200 nanoindenter (Agilent Technologies). Some 6−14 samples were tested for each pillar size. The top surfaces of the 472 and 986 nm diameter nanopillars were gently polished by the ion beam prior to mechanical testing to minimize the roughness of the top surface. This was necessary because in the course of this work we discovered that the surface roughness in the larger diameter nanopillars led to anomalously low stiffnesses which, in turn, could cause an underestimate of the flow stress (see Supporting Information). The elastic deformation of the substrate underneath the loaded pillar was accounted for by applying the Sneddon correction.[4] The yield stress of bulk nanocrystalline Pt was obtained from nanoindentation into the electrodeposited nanocrystalline film using a sharp Berkovich tip (G200, Agilent Technologies; Synton-MDP). Seven indents, separated by at least 15 μm, were performed to a depth of ~150 nm (<10% of the film thickness to minimize substrate effects) and at a constant strain rate of 0.001/s.[35] The hardness and modulus were determined based upon the Oliver−Pharr method.[35] The substrate consisted of a 100 nm thick gold film (which served as the conducting seed layer for electroplating) on a silicon wafer. The elastic mismatch between Pt and Au was accounted for by removing the additional compliance of the gold film. This compliance was determined by assuming uniaxial compression of a gold slab with a circular contact area with a radius equivalent to the thickness of the Pt thin film.[36]

Figure 3A shows several representative stress−strain curves for nanopillars with $60 \leq D \leq 986$ nm. Plastic flow in the $D = 60 \pm 2$ nm and 113 ± 1 nm nanopillars appears as a series of small, convex undulations in the monotonically increasing stress−strain curve envelope. Similar convex segments, albeit with smaller amplitudes, were also observed in the stress−strain curves of the $D = 270 \pm 7$ nm and 472 ± 10 nm nanopillars. Such stochastic, nonsmooth behavior was not visible in the largest diameter (986 ± 18 nm) samples; the behavior of which closely resembles that of bulk nanocrystalline metals.[37,38] The described stress−strain signatures were consistently reproduced by each of the 6−14 samples tested for each diameter. This type of a discrete-to-smooth transition was previously observed in the compressive response of nanocrystalline Ni-4%W nanopillars of similar diameters with 60 nm grains.[16] The pillar morphology remained nearly cylindrical up to compressive strains of 10−15% (Figures 5F−I), after which failure occurred via buckling, similar to that observed by Jahed et al.[18]

A dramatic 36% weakening in the 60 nm sized samples was observed, whereas larger samples exhibited flow stresses indistinguishable (within the uncertainty of the measurements) from the bulk. The dependence of strength on nanopillar diameter was quantified by identifying yield from the stress−strain curve using the 0.2% offset method. These yield stresses are plotted in Figure 3B as a function of pillar diameter. In all cases, yield occurred before the onset of buckling but after establishing full contact between the pillar and the indenter, as identified by the harmonic continuous stiffness measurement

dx.doi.org/10.1021/nl3036993 | Nano Lett. 2012, 12, 6385−6392

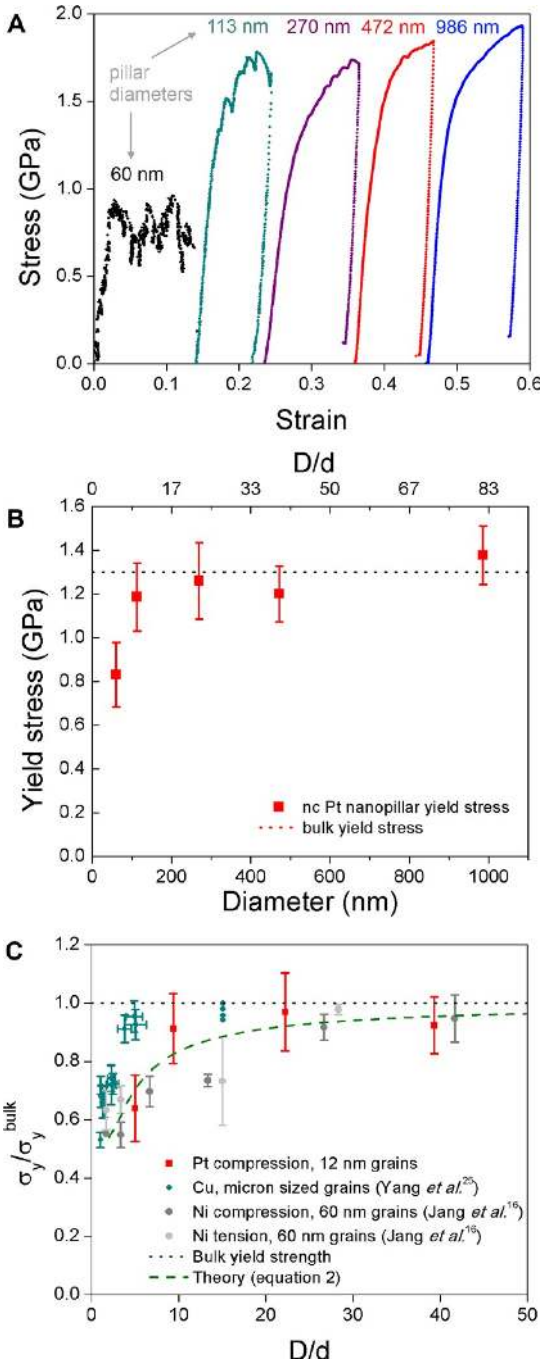

Figure 3. True stress–true strain data for experimentally compressed nanocrystalline Pt pillars. (A) Representative stress–strain curves and (B) 0.2% offset yield strengths for different pillar sizes. (C) The yield strength of the Pt pillars as normalized by the bulk nanocrystalline yield strength compared with that for nanocrystalline Ni pillars with 60 nm grains and polycrystalline Cu wires with micrometer-scale grains near the "smaller is weaker" transition.

(CSM) for every compression test.[4] The bulk yield strength was obtained via nanoindentation of an electrodeposited nanocrystalline Pt film using

$$H = C \times \sigma_y \quad (1)$$

where H is the measured indentation hardness and C is the Tabor factor with a value of 3. Bulk yield stress (σ_y) was determined to be 1.3 ± 0.1 GPa. The yield strength of a Pt thin film with grain size d = 25 nm loaded in tension was reported to be ~1.6 GPa; i.e., a value 40% higher than the yield strengths measured in this work.[39] The lower strengths of the 12-nm-grained samples found in this work as compared with those from the larger-grained Pt films provide further evidence of the inverse Hall-Petch effect and are consistent with reports on similar nanoscale grain sizes in Ni and Cu.[38,40] Figure 3C shows the yield strengths, normalized by the measured bulk yield strength, plotted against D/d. All of the samples other than those with a 60 nm diameter showed normalized strengths within 9% of bulk yield strength. This suggests that a transition from a size-independent to a size-dependent, "smaller is weaker" regime occurs with decreasing D/d.

Figure 3C compares the observed size dependence in nanocrystalline Pt nanopillars to that of nanocrystalline Ni and microcrystalline Cu.[16,25] In all three cases, the yield stress asymptotically approaches the bulk value with increasing D/d and shows pronounced weakening with decreasing D/d below some material-dependent value. Nanocrystalline Ni data for d = 60 nm showed size-dependent weakening at a D/d of 15–30, nanocrystalline Pt with d = 12 nm grains (present work) weakened at a D/d between 5 and 10, and microcrystalline Cu with d = 2–24 μm grains weakened at a D/d of ~2. The observed 37% weakening in the strength of nanocrystalline Ni occurred over a D/d range of about 25, while a similar degree of weakening occurred in nanocrystalline Pt and microcrystalline Cu over a much smaller D/d range of ~4. This implies that D/d does not completely define where the transition to "smaller is weaker" occurs; additional factors such as the intrinsic materials properties of the metals and the absolute grain size may play important roles as well. This result agrees well with previous studies of macroscopic polycrystals with few grains, where weakening was observed below D/d of 3–20 and where both the critical value of D/d and the weakening rate were functions of the material, grain size and geometry, and sample geometry.[22−24]

We performed a series of molecular dynamics (MD) simulations to gain further insight into the observed compressive behavior of nanocrystalline Pt nanopillars. Simulation samples were constructed by first forming a rectangular prism with dimensions of 64 × 64 × 206 nm, containing 648 grains with an average grain diameter of d = 14 nm and random crystallographic orientations. The polycrystalline nanopillar samples were created using the Voronoi procedure on the periodic prism unit cell, as described in Wu et al.[41] Two cylindrical nanopillars of diameters D = 43 and 64 nm and lengths of 206 nm were cut from the rectangular prism. Following the same procedure, two smaller cylindrical nanopillars (D = 22 and 32 nm and length of 103 nm) were cut from a shorter rectangular prism (64 × 64 × 103 nm). These nanopillars contained ~2.5–44 million atoms and had a D/d between 1.5 and 4.6, with aspect ratios comparable to those in the experiment.

The MD simulations were performed using the Large-scale Atomic/Molecular Massively Parallel Simulator[42] (LAMMPS) and a Pt embedded atom method (EAM) interatomic potential.[43] Periodic boundary conditions were imposed along the pillar in the axial direction. The simulation samples were equilibrated at 300 K.[44] Subsequently, a uniaxial compressive displacement was applied parallel to the nanopillar axis at the same temperature and at a constant true strain rate of 0.1/ns. The compressive strength of the corresponding bulk nanocrystalline Pt was determined by compressing the rectangular

dx.doi.org/10.1021/nl3036993 | Nano Lett. 2012, 12, 6385–6392

prism (with periodic boundary conditions) in its long axis direction. During compression, constant temperature and zero lateral normal stresses (in the periodic rectangular prism) were maintained using the Nose–Hoover temperature thermo/barostat.[45−48]

The engineering stress–engineering strain curves for the Pt nanopillars from the MD simulations are shown in Figure 4A.

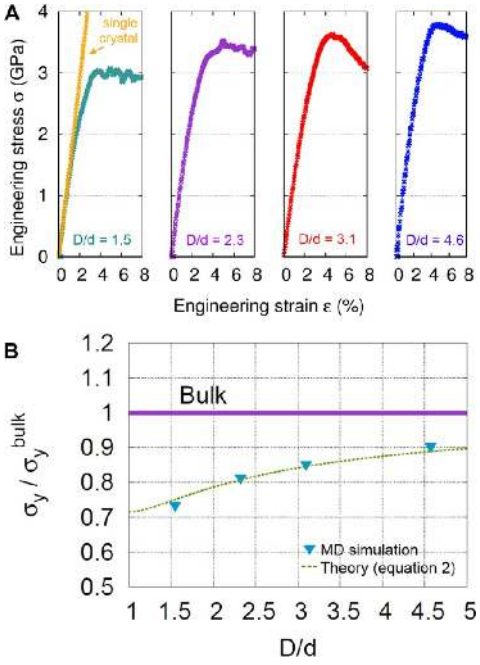

Figure 4. Yield behavior of Pt nanocrystalline nanopillars with a grain size of 12 nm as determined from the MD simulations. (A) Stress–strain curves of nanocrystalline samples with varying D/d, and single crystal sample with pillar size identical to nanocrystalline sample with D/d = 1.5. (B) 1% offset yield stress normalized by the bulk nanocrystalline sample yield stress.

Figure 4B shows the yield stresses normalized by the bulk yield strength as a function of D/d. These yield stresses were extracted from the stress–strain data at a 1% strain offset because the MD samples were nonlinear elastic at 0.2% strain offset. A [001]-oriented single crystal with the same sample size as the D/d = 1.5 pillar was loaded in the same way as for the nanocrystalline samples. The resulting single-crystal stress–strain curve is nearly linear in the range of strain in which the nanocrystalline samples were nonlinear elastic (overlaid on the D/d = 1.5 stress–strain curve in Figure 4A). We conclude that the nonlinear elasticity in the nanocrystalline samples is due to grain boundary sliding rather than being an artifact of the chosen EAM potential. The yield stresses, normalized by their bulk nanocrystalline counterparts, were 75% (D/d = 1.5), 81% (D/d = 2.3), 85% (D/d = 3.1), and 90% (D/d = 4.6) of the corresponding bulk value. For $2.3 \leq D/d \leq 4.6$, a 50% increase in pillar diameter was accompanied by only a 9% increase in the yield strength, indicating that the yield strength became insensitive to D/d above 5. Oscillations were apparent in the plastic region of the stress–strain curves for D/d = 1.5 and 2.3 samples. Similarly to the experiments, these oscillations became increasingly muted with increasing sample size.

These findings show excellent qualitative agreement between experiments and simulations. Quantitatively, however, there are differences. At $D/d \sim 5$, the nanopillars in the experiments showed a large and abrupt decrease in yield strength compared with the bulk value, while the nanopillars in the simulations showed a more gradual decrease with decreasing pillar diameter. The difference between the experiment and the simulation may be attributed to one or more of the following reasons. First, when the average $D/d \sim 5$, the variation in grain size within the experimental polycrystal may result in regions where the local D/d is significantly less than 5, leading to early yield at these locations. Hence, at small D/d, the use of an average D/d may be insufficient to interpret the yield strength. The experimental polycrystalline nanopillars may also contain grain boundaries with a statistical distribution of strengths. Among this distribution would be relatively weaker grain boundaries and their associated triple junctions. A pillar with small D/d that contains one of these "weak link" grain boundaries is less likely to contain many other grain boundaries and its yield strength may be decreased because of earlier deformation at the weaker grain boundary. Second, the simulations were performed at a much higher strain rate than used in the experiments. This resulted in a higher flow stress in the simulations as compared with the experiments, which may shift the balance between the different deformation mechanisms.

Our simulations show that the nanopillars initially underwent nonlinear elastic compression, followed by plastic deformation and, subsequently, plastic bending/buckling. Figure 5A–E shows a series of images from the compression of the D = 64 nm nanopillar. The buckling occurred at a compressive strain of ~8% and is clearly visible at 10% and 15% (see Figure 5D and E), consistent with the experimental observations (Figure 5F–I).

A detailed examination of the deformed microstructures revealed that the interior of the nanopillars underwent plastic deformation through dislocation mechanisms. In particular, dislocations were nucleated from grain boundary triple junctions, then rapidly propagated across a grain and absorbed by a grain boundary of the same grain (Figure 6). The deformation behavior in the interior of the nanopillars resembled that observed in the bulk nanocrystalline samples. Near the free surface, however, the deformation was found to be dominated by grain boundary sliding, which led to the formation of small surface steps on the order of atomic spacings at some of the grain boundary/free surface intersections. The grain boundary sliding was found to be of the Rachinger type rather than Lifshitz (diffusional) grain boundary sliding.[49,50] The movement of atoms on grain boundaries and lattice positions was tracked throughout the simulations, and it was found that the amount of lattice atom diffusion toward grain boundaries, as well as grain boundary atom diffusion through grain boundaries, is small, as compared to grain sliding against each other along their boundaries (see Supporting Information). As a result, appreciable stress concentrations are observed at GB triple junctions, which in turn lead to dislocation nucleation at triple junctions. Additionally, most grains do not change shape significantly prior to the yield point. No dislocation activity was seen in these grains up to the plastic yield strain (defined here as 1% plastic strain). The surface steps appeared prior to the nucleation of *any* dislocations in the nanopillar interior. Previously published models for the "smaller is weaker" transition in macroscopic samples may not be applicable to nanocrystalline materials because they attributed the size effect to differences in dislocation activity in surface and

dx.doi.org/10.1021/nl3036993 | *Nano Lett.* 2012, 12, 6385–6392

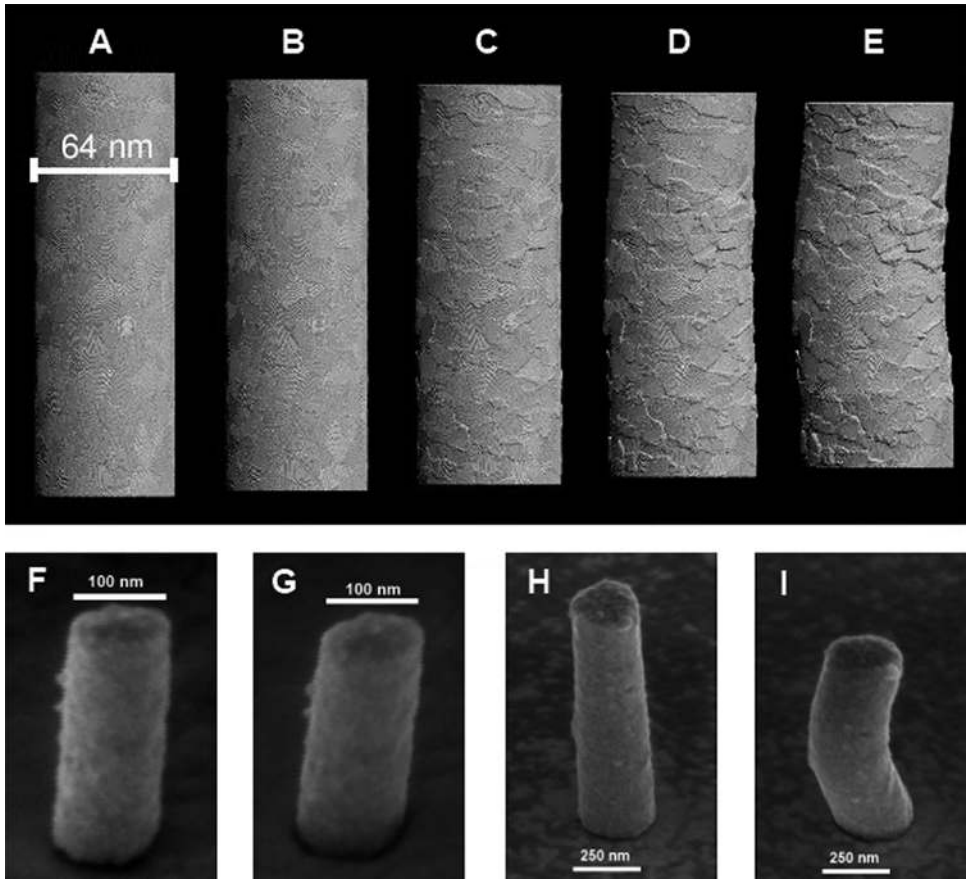

Figure 5. Snapshots from MD simulation showing the progression from (A) 0% strain (undeformed pillar), (B) 3% strain (elastically deformed), (C) 6% strain (plastically deformed), (D) 10% strain (further plastically deformed) to (E) 15% strain (plastically bending). The same deformation modes were observed in experiment: SEM images of a 113 nm pillar at (F) 0% strain (undeformed) and (G) ~10% strain (plastic deformation); a 270 nm pillar at (H) 0% strain (undeformed) and (I) ~25% strain (plastic bending). SEM images were taken at a 52° tilt.

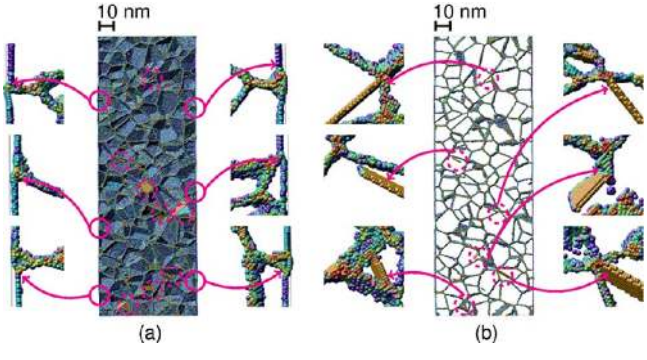

Figure 6. MD simulation of the nanopillar under compressive loading at 4.8% strain. (A) Grain boundary sliding at the surface grains and (B) partial dislocation nucleation at triple junctions and the resulting stacking faults as the partial dislocations propagate through the pillar interior.

interior grains while dislocation activity in nanocrystalline materials may be limited.[25,51,52]

Grain offsets at the surface of nanocrystalline Al and Ni films have previously been measured using atomic/scanning force microscopy.[53−55] Using similar techniques to experimentally confirm the presence of grain offsets on the nanocrystalline Pt nanopillars would show further agreement between experiment and simulation. It is extremely challenging to measure grain offsets at the surface of the pillars because of the complex geometries of these samples and the very small size of the grain offsets predicted by simulation, but this will be explored in future work.

Direct observation of the detailed deformation mechanism during loading of the Pt nanopillars remains an experimental challenge. Hence, atomistic simulations represent an important tool for deducing the operative deformation mechanism, provided that key observations are shown to be consistent with the experimental data. In the present case, both simulations and experiment show (i) a trend of decreasing strength with decreasing nanocrystalline nanopillar diameter, (ii) the strength asymptotically approaches the bulk nanocrystalline material strength with increasing diameter, and (iii) a trend toward an increasingly oscillatory stress−strain curve with decreasing D/d. The simulations demonstrate that, when the pillar diameter (and D/d) was large, only a small fraction of the sample volume deformed via grain boundary sliding (at the boundaries intersecting or near the surface). In this case, the deformation was controlled by the flow properties of the pillar interior, and hence the yield strength of the pillar was similar to that of the bulk nanocrystal. Although the effective flow stress of the grains adjacent to the surface (in this case, flow associated with grain boundary sliding) is lower than those in the pillar interior (dislocation plasticity), the total load carried by the surface region is negligible since the grain diameter is much smaller than the pillar diameter. This also explains why the yield strength approaches its bulk value as the pillar

dx.doi.org/10.1021/nl3036993 | *Nano Lett.* 2012, 12, 6385−6392

diameter increases with fixed grain size. Since the dominant deformation mechanism near the surface is associated with grain boundary sliding, and the flow stress for grain boundary sliding is lower than that associated with bulk nanocrystal dislocation plasticity, it is expected that the transition between these two regimes is responsible for the emergence of a size effect. For the simple case where the material is elastic-ideally plastic and for which the grains in the nanopillar interior have a higher yield strength σ_y^{bulk} than those at the surface where grain boundary sliding (σ_y^s) occurs, the yield strength should scale as:

$$\sigma_y = \sigma_y^{bulk}\left(1 - \frac{d}{D}\right)^2 + \sigma_y^s\left[1 - \left(1 - \frac{d}{D}\right)^2\right] \quad (2)$$

The derivation for this formula can be found in the Supporting Information and Greer et al.[56] In the limit that the grain size is much smaller than the nanopillar diameter ($d/D \to 0$), the yield strength tends to the bulk yield strength as $\sigma_y = \sigma_y^{bulk} - 2d/D(\sigma_y^{bulk} - \sigma_y^s)$. On the other hand, when the nanopillar diameter approaches the grain size, $r = (D - d) \to 0$, the yield strength tends toward the yield strength associated with grain boundary sliding as $\sigma_y = \sigma_y^s + (\sigma_y^{bulk} - \sigma_y^s)r^2/D^2 \approx \sigma_y^s$ to leading order in r/D. Nanocrystalline Pt nanopillar experimental and MD simulation data were fitted to eq 2 (see Figures 3C and 4B), and the value of $\sigma_y^s/\sigma_y^{bulk}$ was found to be 0.54 and 0.72 for experiments and simulations, respectively. This difference between experiment and simulation results may be due to previously discussed issues such as variability in microstructure and differences in the strain rate.

Differing propensities for grain boundary sliding versus partial dislocation nucleation may be responsible for the observed differences in the size-dependence of the yield strength in Pt, Ni, and Cu (Figure 3C). For example, grain boundary sliding resistance and flow properties of bulk nanocrystalline materials may depend, to different extents, on stacking fault energy. Another possible reason is the difference in the microstructures, for example when d is smaller than a critical dislocation half-loop radius, dislocation nucleation in the interior can only occur at large applied stresses; this leads to a dependence on the grain size as well as D/d. Additionally, when the average D/d is small, the variability in the local grain size (and hence D/d) can be large, and yielding will occur by grain boundary sliding along the shortest grain boundary path across the pillar diameter.

In conclusion, a strong sample size dependence in the plastic response of uniaxially compressed Pt nanopillars with 12-nm-sized grains was observed in both experiment and MD simulations. Both experiment and simulation also showed that stochastic, undulating plastic flow was observed for small pillar sizes and continuous, smooth flow at larger pillar sizes. A clear transition to a "smaller is weaker" regime occurred at a $D/d \sim 5$, with the smallest pillars 36% weaker in the experiment and 10% weaker in the MD simulation as compared to bulk nanocrystalline Pt. This transition was found to depend on the absolute grain size and the metal material properties (e.g., stacking fault energy or boundary sliding resistance), as well as the characteristic dimension ratio D/d. MD simulations revealed that the transition in behavior with nanopillar diameter results from the competition between accommodation of the applied load by grain boundary sliding at surface grains and nucleation and propagation of partial dislocations in the interior grains. Grain boundary sliding occurs at surface grains (and causes surface relief) at applied stresses too low for the nucleation of partial dislocations within the pillar interior. Thus, pillars with small D/d yield at a lower stress simply because the fraction of grains that is at the surface increases with decreasing D/d. The present combined experimental and simulation investigation of the mechanical deformation of nanocrystalline Pt nanocylinders provides clear evidence of the role of grain size, materials properties, and sample dimensions in the deformation of metallic nanostructures.

■ ASSOCIATED CONTENT

Supporting Information

Explanation of measurement artifacts, detailed examination of grain boundary sliding, derivation of yield stress formula, and Figures S1–S5. This material is available free of charge via the Internet at http://pubs.acs.org.

■ AUTHOR INFORMATION

Corresponding Author

*E-mail: jrgreer@caltech.edu.

Notes

The authors declare no competing financial interest.

■ ACKNOWLEDGMENTS

J.R.G. and X.W.G. acknowledges support from NSF Career Grant (DMR-0748267) and the Office of Naval Research (N00014-09-1-0883). X.W.G. acknowledges support from the National Defense Science and Engineering Graduate (NDSEG) Fellowship, 32 CFR 168a. X.W.G. and J.R.G. would also like to thank the Kavli Nanoscience Institute at Caltech for support and access to critical cleanroom facilities, Dr. Dongchan Jang for TEM assistance, and Dr. Qiang Guo for electroplating templates.

■ REFERENCES

(1) Hall, E. O. *Proc. Phys. Soc. London, Sect. B* **1951**, *64*, 747.
(2) Petch, N. J. *J. Iron Steel Inst.* **1953**, *174*, 25.
(3) Uchic, M. D.; Dimiduk, D. M.; Florando, J. N.; Nix, W. D. *Science* **2004**, *305*, 986.
(4) Greer, J. R.; Oliver, W. C.; Nix, W. D. *Acta Mater.* **2005**, *53*, 1821.
(5) Uchic, M. D.; Shade, P. A.; Dimiduk, D. M. In *Annual Review of Materials Research*; Annual Reviews: Palo Alto, CA, 2009; Vol. *39*, p 361.
(6) Jennings, A. T.; Burek, M. J.; Greer, J. R. *Phys. Rev. Lett.* **2010**, *104*, 135503.
(7) Buzzi, S.; Dietiker, M.; Kunze, K.; Spolenak, R.; Loffler, J. F. *Philos. Mag.* **2009**, *89*, 869.
(8) Greer, J. R.; De Hosson, J. T. M. *Prog. Mater. Sci.* **2011**, *56*, 654.
(9) Rao, S. I.; Dimiduk, D. M.; Parthasarathy, T. A.; Uchic, M. D.; Tang, M.; Woodward, C. *Acta Mater.* **2008**, *56*, 3245.
(10) Diao, J. K.; Gall, K.; Dunn, M. L.; Zimmerman, J. A. *Acta Mater.* **2006**, *54*, 643.
(11) Dimiduk, D. M.; Woodward, C.; LeSar, R.; Uchic, M. D. *Science* **2006**, *312*, 1188.
(12) Schuster, B. E.; Wei, Q.; Zhang, H.; Ramesh, K. T. *Appl. Phys. Lett.* **2006**, *88*, 103112.
(13) Kunz, A.; Pathak, S.; Greer, J. R. *Acta Mater.* **2011**, *59*, 4416.
(14) Guo, Q.; Greer, J. R. *Scr. Mater.* **2012**, *66*, 272.
(15) Jang, D. C.; Cai, C.; Greer, J. R. *Nano Lett* **2011**, *11*, 1743.
(16) Jang, D. C.; Greer, J. R. *Scr. Mater.* **2011**, *64*, 77.
(17) Rinaldi, A.; Peralta, P.; Friesen, C.; Sieradzki, K. *Acta Mater.* **2008**, *56*, 511.
(18) Jahed, Z.; Jin, S. M.; Burek, M. J.; Tsui, T. Y. *Mater. Sci. Eng., A* **2012**, *542*, 40.
(19) Mara, N. A.; Bhattacharyya, D.; Dickerson, P.; Hoagland, R. G.; Misra, A. *Appl. Phys. Lett.* **2008**, *92*, 231901.

(20) Jang, D.; Li, X.; Gao, H.; Greer, J. R. *Nat. Nanotechnol.* **2012**, *7*, 594.
(21) Lian, J.; Jang, D.; Valdevit, L.; Schaedler, T. A.; Jacobsen, A. J.; Carter, W. B.; Greer, J. R. *Nano Lett.* **2011**, *11*, 4118.
(22) Hansen, N. *Acta Metall.* **1977**, *25*, 863.
(23) Miyazaki, S.; Shibata, K.; Fujita, H. *Acta Metall.* **1979**, *27*, 855.
(24) Janssen, P. J. M.; de Keijser, T. H.; Geers, M. G. D. *Mater. Sci. Eng., A* **2006**, *419*, 238.
(25) Yang, B.; Motz, C.; Rester, M.; Dehm, G. *Philos. Mag.* **2012**, *92*, 3243.
(26) Kumar, K. S.; Van Swygenhoven, H.; Suresh, S. *Acta Mater.* **2003**, *51*, 5743.
(27) Rupert, T. J.; Gianola, D. S.; Gan, Y.; Hemker, K. J. *Science* **2009**, *326*, 1686.
(28) Shan, Z. W.; Stach, E. A.; Wiezorek, J. M. K.; Knapp, J. A.; Follstaedt, D. M.; Mao, S. X. *Science* **2004**, *305*, 654.
(29) Asaro, R. J.; Krysl, P.; Kad, B. *Philos. Mag. Lett.* **2003**, *83*, 733.
(30) Van Swygenhoven, H.; Derlet, P. A. *Phys. Rev. B* **2001**, *64*, 224105.
(31) Tian, N.; Zhou, Z. Y.; Sun, S. G.; Ding, Y.; Wang, Z. L. *Science* **2007**, *316*, 732.
(32) Burek, M. J.; Greer, J. R. *Nano Lett.* **2010**, *10*, 69.
(33) Yarden, T. S.; Joselevich, E. *Nano Lett.* **2010**, *10*, 4742.
(34) Penner, R. M.; Martin, C. R. *Anal. Chem.* **1987**, *59*, 2625.
(35) Oliver, W. C.; Pharr, G. M. *J. Mater. Res.* **1992**, *7*, 1564.
(36) Nix, W. D., Private communication.
(37) Dalla Torre, F.; Van Swygenhoven, H.; Victoria, M. *Acta Mater.* **2002**, *50*, 3957.
(38) Sanders, P. G.; Eastman, J. A.; Weertman, J. R. *Acta Mater.* **1997**, *45*, 4019.
(39) Jonnalagadda, K. N.; Chasiotis, I.; Yagnamurthy, S.; Lambios, J.; Pulskamp, J.; Polcawich, R.; Dubey, M. *Proc. Soc. Exp. Mech.* **2010**, *67*, 25.
(40) Trelewicz, J. R.; Schuh, C. A. *Acta Mater.* **2007**, *55*, 5948.
(41) Wu, Z. X.; Zhang, Y. W.; Srolovitz, D. J. *Acta Mater.* **2011**, *59*, 6890.
(42) Plimpton, S. *J. Comput. Phys.* **1995**, *117*, 1.
(43) Sheng, H. W.; Kramer, M. J.; Cadien, A.; Fujita, T.; Chen, M. W. *Phys. Rev. B* **2011**, *83*, 134118.
(44) Wu, Z. X.; Zhang, Y. W.; Jhon, M. H.; Gao, H. J.; Srolovitz, D. J. *Nano Lett.* **2012**, *12*, 910.
(45) Nose, S. *J. Chem. Phys.* **1984**, *81*, 511.
(46) Nose, S. *Mol. Phys.* **1984**, *52*, 255.
(47) Hoover, W. G. *Phys. Rev. A* **1986**, *34*, 2499.
(48) Melchionna, S.; Ciccotti, G.; Holian, B. L. *Mol. Phys.* **1993**, *78*, 533.
(49) Langdon, T. G. *J. Mater. Sci.* **2006**, *41*, 597.
(50) Li, X. Y.; Wei, Y. J.; Yang, W.; Gao, H. J. *Proc. Natl. Acad. Sci. U.S.A.* **2009**, *106*, 16108.
(51) Molotnikov, A.; Lapovok, R.; Davies, C. H. J.; Cao, W.; Estrin, Y. *Scr. Mater.* **2008**, *59*, 1182.
(52) Malygin, G. A. *Phys. Solid State* **2012**, *54*, 559.
(53) Chinh, N. Q.; Szommer, P.; Horita, Z.; Langdon, T. G. *Adv. Mater.* **2006**, *18*, 34.
(54) Gianola, D. S.; Eberl, C.; Cheng, X. M.; Hemker, K. J. *Adv. Mater.* **2008**, *20*, 303.
(55) Rabkin, E.; Deuschle, J. K.; Baretzky, B. *Acta Mater.* **2010**, *58*, 1589.
(56) Greer, J. R.; Jang, D.; Gu, X. W. *J. Minerals, Metals, Mater. Soc.* **2012**, *64*, 1241.